Nucleic Acids Research, 1998, Vol. 26, No. 14 3323–3332

Thermal stability of DNA

R. D. Blake* and Scott G. Delcourt

Department of Biochemistry, Microbiology and Molecular Biology, University of Maine, Orono, ME 04469-5735, USA

Received April 17, 1998; Revised and Accepted May 18, 1998

ABSTRACT

T_{ij} and ΔH_{ij} for stacking of pair *i* upon *j* in DNA have been obtained over the range 0.034–0.114 M Na^+ from high-resolution melting curves of well-behaved synthetic tandemly repeating inserts in recombinant pN/MCS plasmids. Results are consistent with neighbor-pair thermodynamic additivity, where the stability constant, s_{ij}, for different domains of length N depend quantitatively on the product of stability constants for each individual pair in domains, s_{ij}^N. Unit transition enthalpies with average errors less than ±5%, were determined by analysis of two-state equilibria associated with the melting of internal domains and verified from variations of T_{ij} with [Na^+]. Enthalpies increase with T_{ij}, in close agreement with the empirical function: $\Delta H_{ij} = 52.78 \cdot T_{ij} - 9489$, and in parallel with a smaller increase in ΔS_{ij}. ΔH_{ij} and ΔS_{ij} are in good agreement with the results of an extensive compilation of published ΔH_{cal} and ΔS_{cal} for synthetic and natural DNAs. Neighbor-pair additivity was also observed for (dA · dT)-tracts at melting temperatures; no evidence could be detected of the familiar and unusual structural features that characterize tracts at lower temperatures. The energetic effects of loops were determined from the melting behavior of repeating inserts installed between (G+C)-rich barrier domains in the pN/MCS plasmids. A unique set of values for the cooperativity, loop exponent and stiffness parameters were found applicable to internal domains of all sizes and sequences. Statistical mechanical curves calculated with values of T_{ij}([Na^+]), ΔH_{ij} and these loop parameters are in good agreement with observation.

INTRODUCTION

Differences in energy between stacked G · C and A · T base pairs in polymeric DNAs lead to complex melting profiles (1) that can be observed with high precision by optical methods (2,3). The many sub-transitions in such profiles represent linked temperature standards that provide a high degree of precision for the evaluation of thermodynamic quantities associated with the stability of DNA. We have been involved in carrying out recursive statistical mechanical evaluations of thermodynamic quantities, primarily T_{ij} and ΔH_{ij}, for hydrogen bonding and stacking of the 10 neighbor pairs ***ij*** in model polymeric sequences. Accurate calorimetric ΔH_{ij} have been a special challenge, however, as has been the reconciliation of ΔH_{ij} from oligomeric specimens in high counter-ion concentrations (4–7) to enthalpies from polymeric specimens (8–13), indicating a constant transition entropy (8,12,13). Calorimetric enthalpies have been considerably lower in accuracy than T_{ij} (14–19), so that errors in non-calorimetric ΔH_{ij} determined from T_{ij}, where $\Delta H_{ij} = T_{ij} \cdot \Delta S$ appear small. The magnitudes and order of ΔH_{ij} determined in this way differ from calorimetric values, although they lead to better agreement between experimental and calculated curves over the range 50–100°C (17).

Recent results obtained by Chan *et al*. on an oligomeric specimen with four equi-spaced (dA · dT)-tracts, further complicates the evaluation of thermodynamic quantities (20,21). They find global melting of their specimen to be preceded by a modest two-state transition below 37°C, accompanied by an enthalpic change. These results were interpreted as reflecting a pre-melting structural transition of the (dA · dT)-tracts, from a low-temperature conformational state with bifurcated three-centered hydrogen bonds to a standard B-form at higher temperatures.

This raises questions about (i) the constant entropy assumption; (ii) the applicability of oligomeric ΔH_{ij} to polymeric systems; (iii) the nearest neighbor model; (iv) the precise states of melting; (v) experimental errors and (vi) the different ionic strength conditions used in the evaluation of thermodynamic quantities. The goal of these studies was to respond to some of these questions, revisiting the question of DNA stability, with improved values for T_{ij} and ΔH_{ij} from helix⇆coil transition equilibria, including an examination of the dependence of T_{AA} on (dA · dT)-tract lengths. Accuracies of our earlier T_{ij} would undoubtedly have been higher with specimens of greater bias in neighbor frequencies, providing a more sensitive test of thermodynamic additivity. Neighbor-pair stabilities have been measured in this study with model synthetic domains in polymeric specimens, synthesized with biased neighbor pair frequencies and installed in a modified pBR322 plasmid for cloning purposes. The focus has been limited to the dissociation of helix ends and internal domains, since these two classes of structural transition involve the parameter most associated with all five classes that occur during melting (22).

MATERIALS AND METHODS

DNA specimens

The principal specimens used in these studies were plasmid DNAs constructed in this laboratory as previously described (23) by established procedures (24). These plasmids contain a

*To whom correspondence should be addressed. Tel: +1 413 458 1835; Fax: +1 413 597 4116; Email: blake@maine.maine.edu

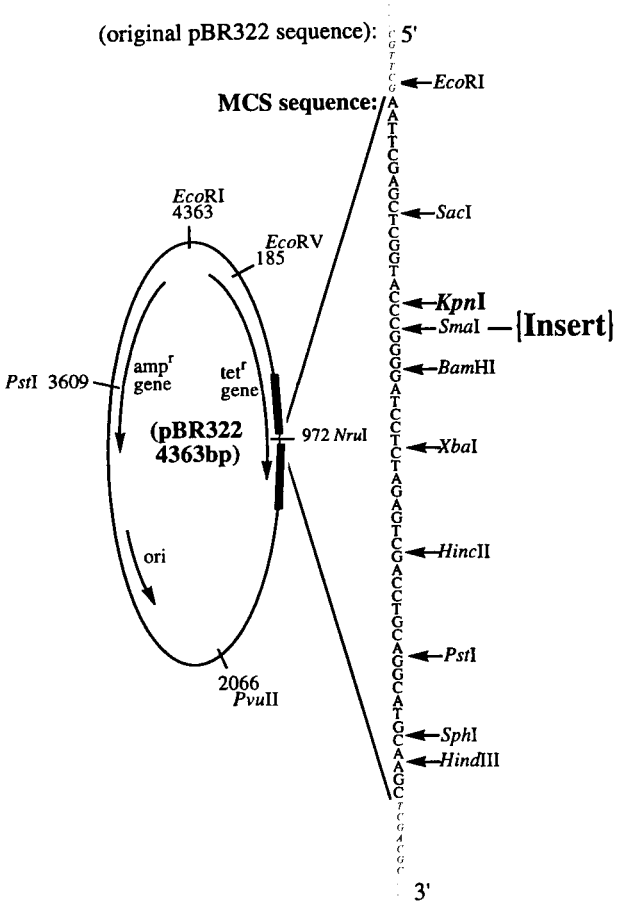

Figure 1. Sequence map of the pN/MCS plasmids used in this study. A 54 bp multiple cloning sequence (MCS) containing recognition sequences for 10 restriction enzymes, was installed at the unique *Nru*I locus of pBR322, between two (G+C)-rich domains denoted by the heavy lines. Tandemly repetitive sequences described in Table 1a and b were then inserted at the *Sma*I locus of the MCS.

repetitive sequence at a site in the plasmid exhibiting favorable energetic characteristics. As shown in Figure 1, the preparation of the pN/MCS plasmids first involved the installation at the unique *Nru*I locus (972) of pBR322 of a 54 bp multiple cloning sequence (MCS) with recognition sites for 10 restriction enzymes. Following this, the repetitive sequences described in Table 1a and b were inserted at the unique *Sma*I locus of the MCS. This locus is immediately adjacent to a unique *Kpn*I recognition sequence in the MCS, and 803 bp away from an *Eco*RV sequence, both sites used to linearize the plasmid in preparation for melting. Numerous model plasmids containing unique or oligomeric repeating sequences such as the homologous series: [AAGTT-GAAC(A)$_M$T]$_N$AAGTTG, where $6 \geq M \geq 0$ and $57 \geq N \geq 16$, were prepared in similar fashion. Repeat lengths are short to ensure biased frequencies of neighbor pairs, but long enough to discourage mismatched alignments at equilibrium temperatures during melting.

In the preparation of oligomer repeats, the residues of *N*-base oligonucleotides were first paired with the residues of complementary overlaps of (*N*/2)-base oligonucleotides, and then ligated using T4 DNA ligase to generate tandemly repeating duplexes of 100–1000 bp. These duplexes were size fractionated on low-melting agarose, and fragments >200 bp removed from the gel and made blunt with Klenow enzyme. The resulting DNA was ligated into pN/MCS at the *Sma*I locus of the MCS. In preparation for insertion of the repetitive elements, pN/MCS plasmid was restricted at the unique *Sma*I site and digested with bacterial alkaline phosphatase to remove the terminal 5′ phosphate groups to prevent vector recircularization during the ligation step. The phosphatase was inactivated by the addition of SDS, followed by phenol extraction. Plasmid DNA was then precipitated and ligated to the repetitive DNA at an insert:vector mole ratio of >10:1 using T4 DNA ligase.

Circular recombinant plasmids were introduced into *Escherichia coli* HB101 or SURE™ cells, and transformed cells were selected on agar containing ampicillin. Cells containing plasmid were grown in 1 l of ampicillin-selective LB broth, and amplified by the addition of chloramphenicol. Cells were lysed in alkaline SDS, and the plasmid precipitated from the lysate in isopropanol. Residual contaminates in crude plasmid DNA lead to non-linear baselines in the high resolution melting curves, and could not be removed by any of the convenient filtration procedures that are commercially available. Two successive CsCl gradients were required to achieve a suitable state of purity. The repetitive inserts were checked by double-stranded sequencing over the insert region by the dideoxy chain-termination method (25), as well as by electrophoretic mobility.

Equilibrium melting curves

High resolution derivative melting curves were obtained by the difference-approximation method (26,27), with a modified double-beam ratio-recording spectrophotometer (Cary). The finite difference method involves the approximation of a derivative $dA_{\lambda(nm)}/dT$ by its differential $\Delta A_{\lambda(nm)}/\Delta T$, with analytical reconstruction of the true derivative achieved as previously described (26). Temperatures were ramped at 6°C/h, which has been shown to provide equilibrium melting of most domains. Slower rates lead to a significant increase in thermal degradation, particularly of single-stranded coil regions (28). For this reason, specimens were never re-melted; instead, replicate experiments were always carried out on fresh aliquots of the same or new preparations. The distribution of (G+C) compositions and sizes of domains responsible for sub-transitions were obtained by spectral decomposition of melting curves obtained at 260, 270 and 282 nm, where the ratios of derivative extinction coefficients for A·T and G·C pairs, $d\varepsilon_{A\cdot T}/d\varepsilon_{G\cdot C}$, are 4.31, 1.00 and 0.120, respectively (27).

Approximately 1 µg of commercial poly(dA·dT) (Sigma) of mean length >20 000 bp was added to all specimens before melting, to serve as secondary standard of solvent conditions. The complete melting of this synthetic DNA takes place within ±0.07°, with melting temperatures given by the relationship:

$$T_m^{poly(dA\cdot dT)} = 19.07 \log_{10}[Na^+] + 86.87°C \quad \mathbf{1}$$

Solvent

The solvent consisted of the specified [Na^+] in the form of NaCl, plus 0.005 M Na-cacodylate and 0.2 mM Na-EDTA (pH 6.85).

van't Hoff enthalpies

Enthalpies associated with conformational changes in DNA were determined by non-linear regression analysis of first derivative van't Hoff transition equilibria (23) over the entire transition regions of isolated curves for insert sequences, as previously described. The advantage of this method is its high degree of sensitivity, where excellent results can be obtained on <50 μg DNA. The disadvantage is that accurate knowledge of the states of equilibria are determined indirectly, which can be problematic. Denaturation is a complex piecemeal process, with sub-transitions spread over a 15–20° range, emanating from micro-domains of a few base pairs to macro-domains of >500. All have different stabilities and many overlap one another (17), and therefore it can be difficult to determine the states of equilibria for individual transitions. The difficulty can be circumvented, however, by constructing plasmid DNAs, such as the pN/MCS-series described above, that harbor large, discrete domains of sharply-melting oligonucleotide repetitive elements. The equilibrium denaturation of these domains can be isolated from the background contributions of nearby transitions by subtracting denaturation profiles of plasmids without the insert from those that have it (17,23).

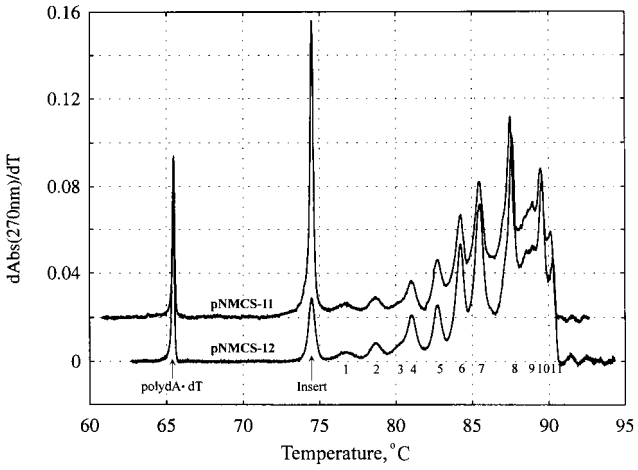

Figure 2. Illustrative melting curves of pN/MCS11 and pN/MCS12 DNA. These curves were obtained from the derivative of the loss of hypochromicity at 270 nm; in the standard buffer: 0.005 M Na-cacodylate, 0.2 mM Na-EDTA, 0.074 M NaCl, pH 6.85. The insert sequence in these plasmids was [AAGTT-GAACAAAT]$_N$AAGTTG, where N = 57 in pN/MCS11 and 16 in pN/MCS12.

RESULTS

Domain stability and T_{ij} in the standard buffer (0.075 M Na^+)

Dissociation of DNA takes place in a piecemeal fashion with increasing temperature. Helical segments or domains of variable sizes dissociate in a cooperative fashion by one of five types of sub-transition depending on where the domain occurs (22). Illustrative 270 nm curves of pN/MCS-11 and pN/MCS-12 DNA in the standard buffer are shown in Figure 2. Both show 13 distinct peaks, 12 that originate from the plasmid. Each peak or shoulder generally does not reflect the melting of a single domain, but consists of several sub-transitions closely spaced in temperature. The first, very sharp transition at 65.45° is due to the melting of poly(dA·dT), added to all DNA specimens as a convenient marker and secondary standard of solvent conditions. The melting of this synthetic homoduplex is sharp and particularly sensitive to the effects of ionic strength. It's half-width is only 0.067 ± 0.007°, while T_M of replicate experiments vary by less than ±0.02°. This means T_M of plasmid transitions obtained together in the same ionic environment can be determined with similar precision. Sensitivities of T_M to variations in base composition and ionic strengths are therefore limited only by knowledge of the sequences involved.

Curves of pN/MCS11 and pN/MCS12 in Figure 2 melt over a 15° range, where base compositions of domains contributing to sub-transitions vary between 0.23 and 0.71F_{GC}. The insert in these plasmids: [AAGTTGAACAAAT]$_N$AAGTTG, with a (G+C) content of only 0.23, was installed at the *Sma*I locus of the MCS. This locus splits a large, relatively (G+C)-rich domain in two, creating two (G+C)-rich boundaries that serve as energetic barriers to further melting of inserts. The helix⇆coil sub-transitions of these barrier domains, represented by heavy lines in Figure 1, occur at the higher temperatures corresponding to peaks labeled 10 and 11.

The curves in this figure were obtained from plasmid DNAs linearized at the unique *Kpn*I sequence in the MCS in preparation for melting. The recognition sequence for this enzyme (GGTACC) is immediately adjacent to the insert, which is substantially lower in (G+C) content than the adjacent barrier domain, so that inserts in *Kpn*I-cut plasmids melt from one end of the DNA. The first sub-transitions emanating from both plasmids in Figure 2 are for the insert. In pN/MCS11, the insert has N = 57 repeats for a total domain length of 747 bp. The T_M for this insert is 74.49°C. In pN/MCS12, N = 16 for a length of 214 bp, with a T_M = 74.48°C. As given in Table 1a, *Kpn*I-cut pN/MCS10 with the same repeat sequence of an intermediate length (500 bp) melts at 74.42°C. Thus, T_M are the same for all three repetitive inserts (74.46 ± 0.03°C), indicating thermodynamic additivity and the absence of any extraordinary long-range energetic effects associated with domain lengths >214 bp. The same is true of other repetitive inserts of matching sequence in Table 1a, in quantitative agreement with the long-held assumption that the helix⇆coil equilibrium or stability constant for an entire domain of length N depends on the product of stability constants for the individual pairs in the domain, S_{ij}^N. Also, when transitions are followed at 270 nm where the dissociation of A·T base pairs contributes the same as G·C pairs (27), the integrated areas under these sub-transitions are proportional to domain length, ±10 bp. The integrated area under the sub-transition for the 747 bp insert in pN/MCS11 in Figure 2 is almost exactly 3.5× larger than for the insert transition in pN/MCS12.

The results in Table 1a give clear indications of the level of precision that can be achieved in T_M of domains. T_{ij} were derived in this study from a large set of linear algebraic expressions for measured T_M of domains, where

$$T_M = \Sigma f_{ij} \cdot T_{ij} \qquad \mathbf{2}$$

and where f_{ij} represents the fractional neighbor pair frequencies in the domain. T_{ij} were determined by Crout's method for LU matrix decomposition (29). The matrix was filed with 35 linear algebraic equations of the type,

$$f_{AA} \cdot T_{AA} + f_{AT} \cdot T_{AT} + f_{TA} \cdot T_{TA} + \ldots\ldots + f_{GG} \cdot T_{GG} = T_M \qquad \mathbf{3}$$

together with selected results from our previous study of domains of quasi-random sequence. T_M for the synthetic homo- and

Table 1a. Dependence of T_M for repetitive insert domains on base sequence, location and size

Plasmid	Insert Sequence	f_{AA} a)	N bp	*End* T_M °C b) Exptal	Calcd	*Loop* T_M °C c)	ΔT_m^{obs} d)	ΔT_m^{calc} e)
pN/MCS1	$[ACTCGGACGA]_{15}ACTCG$		155	88.631		91.941	2.71	2.85
pN/MCS2	$[ACTCGGACGA]_{30}ACTCG$		305	88.833		90.196	1.36	1.38
pN/MCS2	$[ACTCGGACGA]_{30}ACTCG$		305	88.805		-	1.39	1.38
pN/MCS2	$[ACTCGGACGA]_{30}ACTCG$		305	88.747		-	1.45	1.38
pN/MCS5	$[ACTCGGACGA]_{33}ACTCG$		335	88.842		90.081	1.24	1.25
		(NA)		***88.771 ±0.078***	89.207			
pN/MCS10	$[AAGTTGAACAAAT]_{38}AAGTTG$		500	74.418		75.288	0.87	0.83
pN/MCS10	$[AAGTTGAACAAAT]_{38}AAGTTG$		500	-		75.270	0.85	0.83
pN/MCS10	$[AAGTTGAACAAAT]_{38}AAGTTG$		500	-		75.255	0.84	0.83
						75.271 ±0.013		
pN/MCS11	$[AAGTTGAACAAAT]_{57}AAGTTG$		747	74.488		75.028	0.54	0.56
pN/MCS12	$[AAGTTGAACAAAT]_{16}AAGTTG$		214	74.475		76.348	1.87	2.01
pN/MCS12	$[AAGTTGAACAAAT]_{16}AAGTTG$		214	-		76.273	1.80	2.01
		0.385		***74.460 ±0.031***	74.481	***76.311 ±0.038***		
pN/MCS13	$[AAGTTGAACAAAAT]_{17}AAGTTGA$		245	73.894		75.597	1.70	1.74
pN/MCS13	$[AAGTTGAACAAAAT]_{17}AAGTTGA$		245	-		75.564	1.67	1.74
						75.581 ±0.017		
pN/MCS14	$[AAGTTGAACAAAAT]_{14}AAGTTGA$		203	73.895		75.950	2.05	2.12
pN/MCS14	$[AAGTTGAACAAAAT]_{14}AAGTTGA$		203	-		75.983	2.09	2.12
		0.429		***73.894 ±0.0004***	73.917	***75.967 ±0.017***		
pN/MCS3	$[AAGTTGACAT]_{13}AAGTTG$	0.200	135	76.779	76.815	80.355	3.58	3.31
pN/MCS6	$[AAGTTGAACAAT]_{27}AAGTTG$	0.333	330	75.113	75.139	76.385	1.29	1.27
pN/MCS15	$[AGTGACAT]_{36}AGTG$	0.000	292	79.276	79.326	80.603	1.33	1.45
pN/MCS16	$[AAGTTGAACAAAAAT]_{12}AAGTTGA$	*(f)*	187	74.476	74.385	76.547	2.07	2.32
pN/MCS22	$[AAGTTGAACAAAAAAT]_{12}AAGTTGA$		200	73.078	73.048	75.314	2.24	2.16
pN/MCS22	$[AAGTTGAACAAAAAAT]_{12}AAGTTGA$		200	-		75.360	2.28	2.16
pN/MCS22	$[AAGTTGAACAAAAAAT]_{12}AAGTTGA$		200	-		75.336	2.26	2.16
		0.500				***75.337 ±0.019***		

Table 1b. Additional plasmids with repetitive insert domains examined in this study

Plasmid	Insert Sequence	N, bp
pNR6	$[ACTCGGACGA]_{13}CACTCG$	135
pNR7	$[ACTCGGACGA]_{5}CACTCG$	55
pNR8	$[ACTCGGACGA]_{40}CACTCG$	405
pNR9	$[ACTCGGACGA]_{22}CACTCG$	225
pNR10	$[AAGTTGACAT]_{27}CACTCG$	275
pNR11	$[AAGTTGACAT]_{20}CACTCG$	205
pNR12	$[AAGTTGACAT]_{5}CACTCG$	55
pNR13	$[AAGTTGACAT]_{10}CACTCG$	105
pN/MCS4	$[ACTCGGACGA]_{17}ACTCG$	175
pN/MCS7	$[ACTCGGACGA]_{22}ACTCG$	225
pN/MCS8	[0.395F_{GC} lambda fragment at position #36305-36532]	228
pN/MCS17	$(dA{\cdot}dT)_{50}$	50
pN/MCS20	$[AAGTTGAACAAAAAT]_{5}AAGTTGA$	82
pN/MCS21	$[AAGTTGAACAAAAAT]_{8}AAGTTGA$	127
pN/MCS23	$[CGGTGCTCAAAAAATGTAGCAT]_{15}CGGTGCTCAAA$	341
pN/MCS24	$[AAGTTGAACAAAAAT]_{14}AAGTTGA$	217
pGC110	$[GCCCGGGTACCATGGCACGT]_{5}GCCCGGGTAC$	110
pGC230	$[GCCCGGGTACCATGGCACGT]_{11}GCCCGGGTAC$	230
pGC350	$[GCCCGGGTACCATGGCACGT]_{17}GCCCGGGTAC$	350
pGC530	$[GCCCGGGTACCATGGCACGT]_{26}GCCCGGGTAC$	530

copolymer duplexes that were included previously (17), but now suspected of adopting unusual non-B structures or of dissociating through mismatched intermediate states, were excluded and replaced instead with 22 equations for the T_M of repetitive domains in Table 1a and b. The latter were given greater weight in the matrix since neighbor biases in these sequences are greater. Their T_M, sequence assignments and f_{ij} are more accurate; greater confidence could be attributed to specific neighbor pairs.

Values for T_{ij} in the standard buffer are listed in column six of Table 2, where the average error is ±0.22°. They indicate that $T_M = 42.145 \cdot (G+C) + 63.968$, °C, which is in good agreement with equation **8**, from a very large collection of T_M for natural DNAs accrued over the past 35 years: $T_M = 41.971 \cdot (G+C) + 63.981$, °C (19).

Effects of (dA · dT)-tracts

A number of pN/MCS plasmids with repetitive inserts with between 0 and 8 AA or TT neighbor pairs were constructed, including a series with 1–6 (dA · dT) pairs in tracts. These appear in Table 1a, where there is a value for the insert mole fraction of AA plus TT nearest neighbors, f_{AA}, listed in column three. A plot of T_M for repeat domains against f_{AA} shown in Figure 3 is linear with a correlation coefficient of 0.9997 and standard error of ±0.036°. The absence of curvature or deviation supports the application of nearest neighbor additivity for AA (TT) neighbors at the temperatures of these experiments. Moreover, the data extrapolate to a T_{AA} of 66.81° for the pure AA (TT) neighbor, in good agreement with that obtained by LU decomposition, 66.77° (Table 2), but significantly higher than the T_M for poly(dA · dT), 65.45°C. The lower T_M for the polymeric homoduplex probably reflects the increased access of long (dA · dT)-tracts to greater degrees of freedom during melting, with formation of mismatched loops, and thereby a larger transition entropy.

Loop energetics

The formation of internal loops requires sufficient energy to interrupt the helix; to release stacked residues from cooperative neighbor-pair dispersion forces. Moreover, the restoration of helix from N dissociated coil residues of an internal loop involved in a helix⇆coil equilibrium is favored by the proximity of loop residues. In consequence, the stability constant s_{ij}^N, is weighted by a cooperativity parameter, σ_c, and loop function for the greater probability of closure:

$$S_{ij}^{N+1} \cdot \sigma_c \cdot f(N) \qquad \mathbf{4}$$

Table 2a. Nearest stacked and paired neighbour energies

	5′ *i* 3′ / 3′ *j* 5′	$\frac{dT_{ij}}{d\log[Na^+]}$ °C/K	$T_{ij}^{1.0M\text{-}Na+}$ °C[a]	$T_{ij}^{1.0M\text{-}Na+}$ °K[a]	$T_{ij}^{0.0745M\text{-}Na+}$ °C	ΔH_{ij}[b]	ΔS_{ij}[c]	$\Delta H_{cal,ij}$[b,d]	$\Delta S_{cal,ij}$[c,d]
1	T·A / A·T	22.08	79.47	352.63	54.58	7.81	23.83	7.78	23.73
2	A·T / A·T	19.78	89.08	362.24	66.77	8.45	24.86	8.18	24.02
3	A·T / T·A	19.19	89.38	362.54	67.75	8.50	24.94	8.21	24.04
4	C·G / A·T	19.35	89.71	362.93	67.95	8.51	24.96	8.21	24.04
5	A·T / G·C	17.30	98.49	371.65	78.98	9.10	25.83	8.57	24.30
6	G·C / A·T	16.94	105.09	378.25	85.98	9.47	26.36	8.80	24.47
7	C·G / G·C	16.01	105.28	378.44	87.23	9.53	26.45	8.84	24.50
8	G·C / G·C	14.18	118.49	391.65	102.50	10.34	27.52	9.34	24.86
9	A·T / C·G	13.71	121.17	394.33	105.71	10.51	27.73	9.45	24.94
10	G·C / C·G	10.21	143.73	416.89	132.22	11.91	29.37	10.31	25.56

Table 2b. Free energy differences between (*ij*) and the mean for (*i*,*j*)

	$\delta\Delta G_{ij}$ (cal·mol-bp^{-1})				
ref:	(14,15)	(16)	(17)	(18)	(this work)
1	+369	+334	+186	+80.6	+219.6
2	-80	-54	-35	-151.0	-65.6
3	-143	-179	-175	-71.2	-88.5
4	+476	+45	+399	-51.1	+390.7
5	+383	+149	+205	+222.0	+132.7
6	-324	+42	-117	-161.5	-31.0
7	+588	+562	+421	+26.1	+441.7
8	+249	+178	+155	+192.8	+84.5
9	-608	-272	-497	-128.6	-492.5
10	-1016	-632	-726	-373.9	-610.7

a) The uncertainty in $T_{ij}^{0.0745\ M-Na+}$, $(\Phi/n)^{1/2}$, is ±0.22°, and ±0.56° for $T_{ij}^{1.0\ M-Na+}$.
b) Cal·mol *ij*$^{-1}$. The uncertainty in ΔH_{ij} is ±290 cal·mol *ij*$^{-1}$.
c) Cal·mol *ij*-deg^{-1}; in 0.0745 M – Na^+.
d) From equations **14** and **15** (ref. 38).

where

$$f(N) = (N + D)^{-\alpha} \qquad \mathbf{5}$$

and where N is the number of residues in the loop domain, D is an empirical stiffness parameter, and α the loop-closure exponent.

Repetitive domains melt as internal loops when the pN/MCS plasmids are linearized by *Eco*RV, which cuts at position 185, 805 bp away from the insert. The insert is isolated by (G+C)-rich barrier domains on both sides (Fig. 1). T_M for these interior 'loop

a) Mole fraction of (AA + TT) nearest neighbors in the repeat sequence.
b) Circular plasmid DNA linearized by *Kpn*I, immediately adjacent to the repetitive insert domain. Boxed in *End-*T_M denote values for different lengths of the same repetitive sequence, together with the average and standard deviations for all lengths.
c) Circular plasmid DNA linearized by *Eco*RI, 803 bp away from the repetitive insert domain. Boxed in *Loop-*T_M denote values for replicate measurements, together with the average and standard deviation.
d) Experimental $\Delta T_M = T_M^{loop} - T_M^{end}$.
e) Calculated as described in the text.
f) The repeat sequence of this insert was found to be mysteriously corrupted with nine mutations after transformation and amplification in the host cell: three transitions, six transversions and one deletion. The resulting changes in nearest neighbor frequencies led to an increase of 1.4°C in domain T_M over that that would have been expected for the prototypic sequence. The calculated T_M in column six of this table was determined from the observed (mutated) sequence.

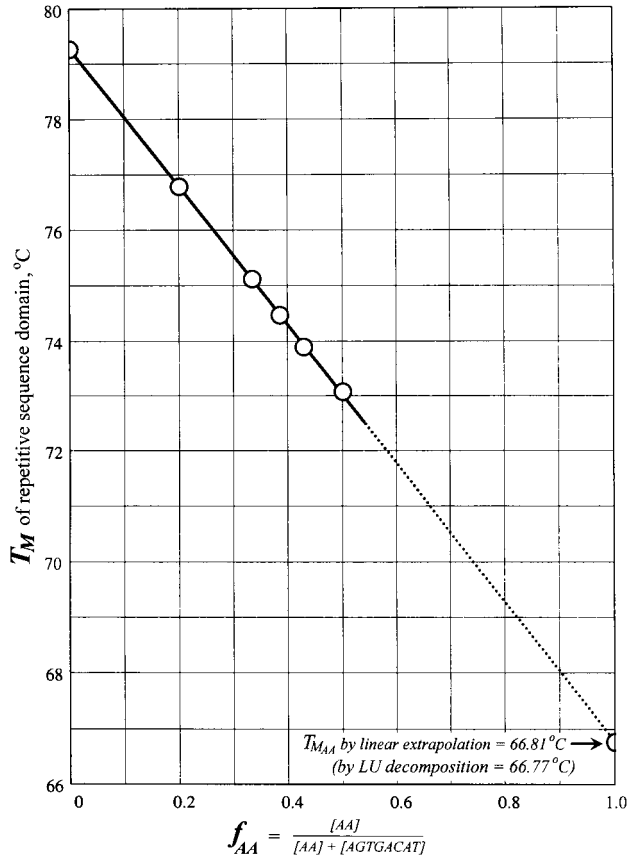

Figure 3. Plot of T_M for repeat domains against the mole fraction of AA (TT) neighbor pairs they contain, f_{AA}.

domains' are higher than for 'end domains' of the same sequence, as can be seen in Table 1a. While domain T_M of repetitive inserts positioned at the end of helixes are dependent only on sequence, they are dependent on both sequence and length when positioned internally. Examples of sub-transitions for both the end (*Kpn*I-cut) and loop (*Eco*RV-cut) melting of the 200 bp repetitive insert in pN/MCS22 are plotted together in Figure 4, represented by the (noisy) traces. These two curves, obtained by subtracting the curve for pN/MCS without insert from pN/MCS22 cut by *Kpn*I and *Eco*RV, have T_M of 73.078 and 75.314°C, respectively, for a $\Delta T_M = T_M^{loop} - T_M^{end} = 2.24°$. Assuming weighting factors for loops to be largely if not totally independent of sequence, their dependence on size will be proportional to ΔT_M. A convenient representation of this dependence for all 22 independent measurements of ΔT_M (Table 1a) is seen with the data points in Figure 5, plotted against *1/N*.

As seen in equation **4**, the evaluation of cooperativity and loop parameters requires knowledge of the stability constants, and thereby, of both transition enthalpies and entropies:

$$s_{ij} = exp(-\Delta G_{ij}/RT) = exp[(-\Delta H_{ij} + T \cdot \Delta S_{ij})/RT] \quad \mathbf{6}$$

where ***ij*** represents each of the 10 neighbor pairs.

Transition enthalpies

Transition enthalpies were determined in this study as described previously (23), by analysis of two-state equilibria associated with

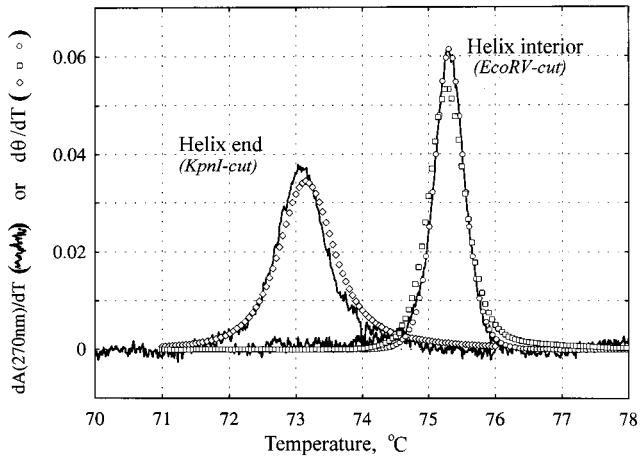

Figure 4. Transitions of the sequence $[AAGTTGAACAAAAAAT]_{12}$AAGTTGA in pN/MCS22 when situated at the *end* and interior (*loop*) of the linearized plasmid DNA, are plotted together in this figure. The experimental curves are represented by the continuous traces. Curves represented by open diamonds (◇) and squares (□), were calculated for *end* and *loop* melting, respectively, by a statistical mechanical routine described in the text. Values for parameters in this routine were taken from Table 2 and the text. The curve represented by open circles (○) was obtained by the van't Hoff cosh equation (22) for two-state transitions, with parameters determined by least-squares regression fit to the experimental loop curve: N = 187 bp, $\Delta\overline{H}_M$ = 8.33 kcal/mol bp, and T_M = 75.34°C.

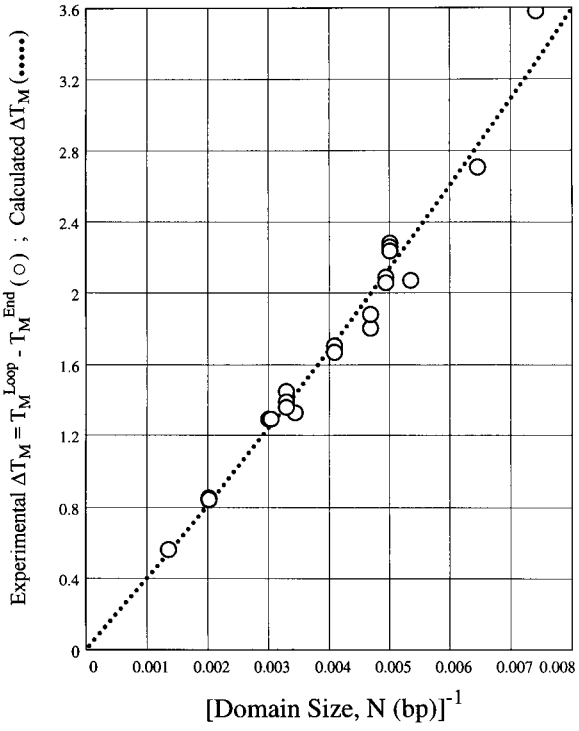

Figure 5. Plot of ΔT_M $T_M{}^{loop} - T_M{}^{end}$ against the reciprocal of the loop domain size, 1/*N*. Experimental results are represented by the open circles, and listed in Table 1a. The dotted line was calculated with the following values in the statistical mechanical routine: $\sigma_c = 1.26 \times 10^{-5}$, D = 1, α = 1.75.

the melting of internal domains. The repetitive domains, locked in between two stable (G+C)-rich neighboring domains, are shown to melt in two-state fashion by several criteria when linearization is catalyzed by *Eco*RV, forcing domains to melt as a closed loop. The

example of the two-state transition for the 0.23 (G+C), 200 bp repetitive insert domain in pN/MCS22 is represented by the sharper, higher temperature transition in Figure 4.

The overall transition enthalpy for this domain, ΔH^{total}, was determined by least-squares fit of the three-parameter van't Hoff 'cosh' equation to the experimental curve in Figure 4 (Materials and Methods). The fit over the full 74.0–76.5°C temperature range, represented by the open circles, gave a $\Delta H^{total} = 1.541 \pm 0.044 \times 10^6$ cal/mol bp. A value of 1.587×10^6 cal/mol bp was obtained over the central 0.8° region, consistent with two-state melting and negligible heat capacity differences between initial and final states. The residuals were small ($\pm 0.00021 A_{270nm}$) and uniformly distributed, consistent with two-state behavior. Transition enthalpies determined previously in this fashion (22), were shown to be within ±3% for the same repetitive sequence differing by 250% in length, while further indications of two-state behavior were confirmed by statistical thermodynamic analyses. The average integrated area under the insert loop sub-transition of pN/MCS22 (Fig. 4) from three measurements on different preparations indicated $N = 187 \pm 7$ bp over the transition region, so that the mean unit enthalpy, $\overline{\Delta H} = [\Delta H^{total}/(N + 1)] = 8325 \pm 380$ cal/mol bp. Lengths of domains from sequence analysis and from integrated areas during melting were confirmed by statistical-mechanical simulations (below).

Average errors of ΔH_{ij} determined from transition equilibria are approximately ±5%, larger for domains of high $f_{(G+C)}$. Since errors in T_{ij} are >10-fold smaller than ΔH_{ij}, the latter were tested against the [Na^+] dependence of T_{ij}, which varies with ΔH_{ij}.

Dependence on [Na^+]

Determinations of T_{ij} in different [Na^+] were carried out to expand the range of applicability of these quantities, as well as confirm values of ΔH_{ij}. The effects of [Na^+] on stability is given by the Marmur–Schildkraut–Doty equation (30,31):

$$T_M\,(^\circ C) = 193.67 - (3.09 - f_{(G+C)})(34.47 - 6.52\log[Na^+]) \quad \mathbf{7}$$

determined from a large collection of measured T_M from published and unpublished results acquired over three decades (19). This relationship was determined from the behavior of very large DNAs and large mixtures of DNAs of different overall base compositions [$f_{(G+C)}$], and is not quantitative for short sequences (≤4000 bp) of biased neighbor frequency.

The Na^+ dependence is caused by the ionic strength-independent condensation of Na^+ to polyanionic DNAs, which have a particularly high negative charge density relative to the single-stranded products. Na^+ are therefore released in large numbers upon melting,

$$DNA_h\text{–}r_{Na^+,h} \cdot Na^+ \leftrightarrow DNA_c\text{–}r_{Na^+,c} \cdot Na^+ + \Delta\bar{r}_{Na^+} \cdot Na^+ \quad \mathbf{8}$$

Subscripts denote helix (h) and coil (c) states, and $\Delta\bar{r}_{Na^+} = \bar{r}_{Na^+,h} - \bar{r}_{Na^+,c}$ the number of Na^+ counterions released from association with the average-sized cooperatively melting domain. T_M of insert domains were measured over the range 0.0344–0.1139 M Na^+, and T_{ij} determined as described above for the standard buffer, and plotted against log[Na^+]. Values for the slopes, $dT_{ij}/d\log[Na^+]$, and intercepts, $T_{ij}^{1.0\ M-Na^+}$, for these linear plots are given in columns three and four of Table 2a.

T_{ij} increase at different rates with [Na^+]. The upshot is that curves of DNAs with domains of different fractional base contents, $f_{(G+C)}$, become more compressed with increasing [Na^+]. For example, curves of *Kpn*I-linearized pN/MCS DNA, shown in Figure 6 on a normalizing ($T_M - T$) scale, melt over an increasingly smaller temperature range with increasing [Na^+]. The compression, which is most evident in the melting of the poly(dA·dT) marker, is inherent in expression **7**, where the derivative of T_M with respect to log[Na^+] yields a value of 20.15° per decade change in [Na^+] when $f_{(G+C)} = 0.0$, but only 13.63° when $f_{(G+C)} = 1.0$. Besides increases in T_M, melting occurs over smaller temperature ranges with increasing [Na^+].

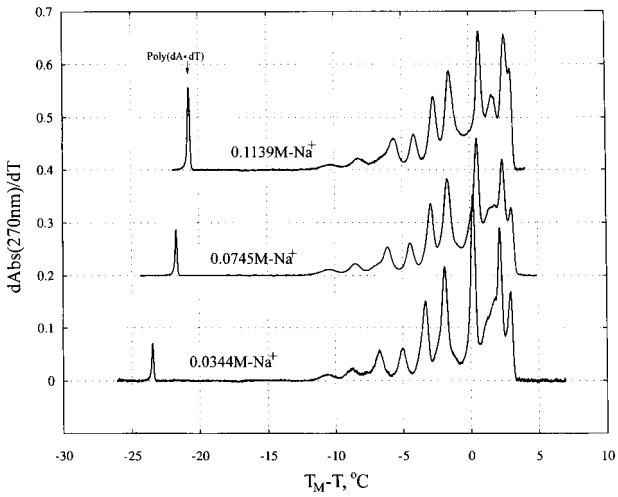

Figure 6. Illustrative melting curves of pN/MCS DNA (no insert) on a normalizing T_M–T scale, at three different sodium ion concentrations.

The theoretical expression for the derivative is given by the Manning–Record equation (12,32):

$$dT_M/d\log[Na^+] = 2.303[(\alpha RT_M^2)/\Delta\overline{H}_M]\Delta\psi_{Na^+} \quad \mathbf{9}$$

where α is the activity coefficient for Na^+; where $\Delta\psi_{Na^+} = \psi_{Na^+,h} - \psi_{Na^+,c}$ represents the differential ion association parameter for the release (per base) of Na^+ bound to helix and coil states, and where $\Delta\overline{H}_M = 0.5\Sigma f_{ij}\Delta H_{ij}$. ΔH_{ij} are primarily [Na^+]-independent; the effect of [Na^+] on DNA stability being entropic (12,33). For the salt concentrations of these experiments, $\alpha \approx 0.95$, while $\Delta\psi_{Na^+}$ varies from 0.19 when $f_{(G+C)} = 0$ to 0.09 when $f_{(G+C)} = 1.0$ (28). The compression phenomenon arises from this decrease in $\Delta\psi_{Na^+}$ with increasing $f_{(G+C)}$. A large collection of calorimetric enthalpies with accompanying T_M for dissociation of polymeric DNA specimens, indicate that $RT_M^2/\Delta\overline{H}_M$ is constant with a value of 55 ± 2 (12). A value of 54 ± 0.2 for $RT_{ij}^2/0.5\Delta H_{ij}$, was obtained over the range 0.03 M < [Na^+] < 0.11 M with values of T_{ij} and ΔH_{ij} from Table 2a.

$dT_M/d\log[Na^+]$ and $dT_{ij}/d\log[Na^+]$ are plotted in Figure 7 against T_M^2 and T_{ij}^2 (in standard buffer), respectively, in accordance with equation **9**. Open circles denote $dT_{ij}/d\log[Na^+]$ (Table 2a), and filled circles $dT_M/d\log[Na^+]$ for transition peaks from the plasmid. The two sets of data are in good agreement with one another. The dotted curve through data points was produced by equation **9** with values for $\Delta\overline{H}_M = 0.5 \cdot H_{ij} = 0.5 \cdot (52.78 \cdot T_{ij} - 9489)$ and $\Delta\psi_{Na^+} = -0.0011 \cdot T_{ij} + 0.523$ over the range $320 < T_{ij} < 410$°K. ΔS_{ij} in Table 2a were calculated from $\Delta H_{ij}/T_{ij}$, since $\Delta G_{ij} = 0 = \Delta H_{ij} - T_{ij}\Delta S_{ij}$ at T_{ij}.

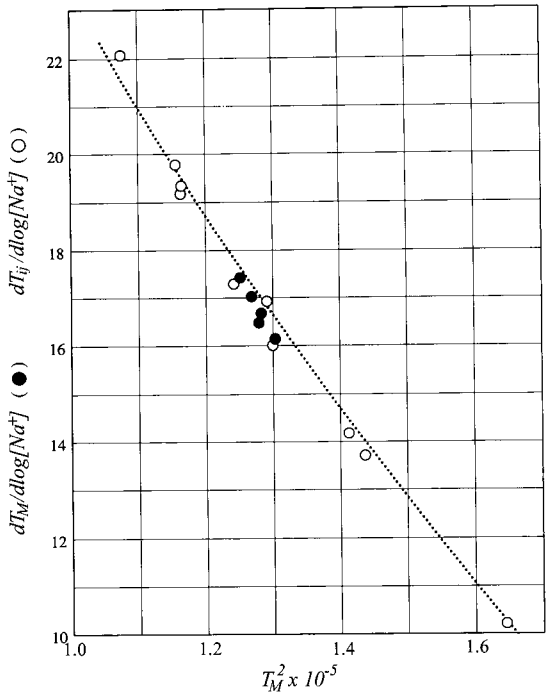

Figure 7. Plots of values for the slopes, $dT_M/dlog[Na^+]$ and $dT_{ij}/dlog[Na^+]$, for the sodium ion dependence of domain and neighbor-pair melting temperatures, respectively, against $T_M^2(T_{ij}^2)$. Closed circles represent slopes for domains, while open circles represent slopes for T_{ij}. The dotted line was calculated with equation **9**, with the following values: $\Delta\overline{H}_M = 0.5 \cdot \Delta H_{ij} = 0.5(52.78 \cdot T_{ij} - 9489)$ and $\Delta\Psi_{Na+} = -0.0011 \cdot T_{ij} + 0.523$ over the range $320 < T_{ij} < 410°K$.

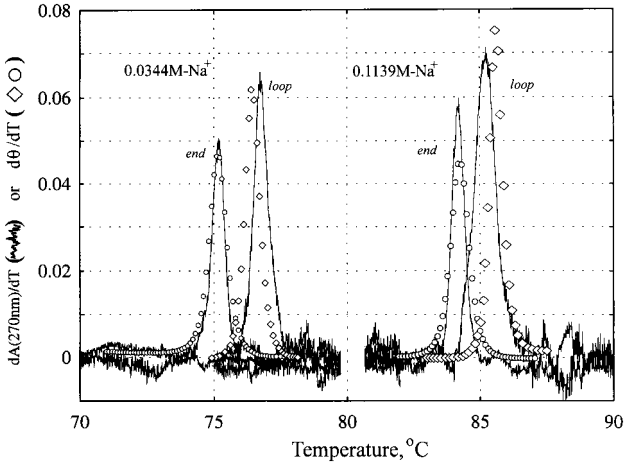

Figure 8. Two transitions of the 228 bp (A+T)-rich λ-DNA insert sequence (36305–36532) in pN/MCS8 when situated at the *end* and interior (*loop*) of the linearized plasmid DNA, at two different sodium ion concentrations, are plotted together in this figure. The four experimental curves are represented by continuous traces. Curves represented by open circles (○) and diamonds (◇), were calculated for *end* and *loop* melting, respectively, by a statistical mechanical routine with values for parameters from Table 2, and the text.

Table 2b lists values for the difference in free energy, $\delta\Delta G_{ij}$, between that for (*ij*) and for the average of like pairs, (*i*,*j*), where,

$$\delta\Delta G_{ij} = \Delta G_{ij} - (\delta\Delta G_i + \delta\Delta G_j)/2 = \delta T_{ij} \cdot \Delta S_{ij}. \qquad \mathbf{10}$$

Statistical thermodynamic analysis

The loop parameters were calculated from equations **4** and **6**, with values for T_{ij}, ΔS_{ij} and ΔH_{ij} from Table 2. Results of $\Delta T_M = T_M^{loop} - T_M^{end}$ in Figure 5 were fit by nonlinear regression to these expressions, from which the following value emerged: $\sigma_c = 1.26 \times 10^{-5}$, when $D = 1$ and $\alpha = 1.75$, represented by the broken curve. All three parameters could not be determined uniquely from these data, therefore values for D and α were assumed (34). Differences between observed and calculated ΔT_M listed in the final two columns of Table 1a are small and within experimental error, suggesting this value for the cooperativity parameter is applicable to loops of all sizes (≥100 bp) and sequences, regardless of (G+C) content.

Transitions were calculated for the pN/MCS plasmid sequences as previously described (17,22). Curves are represented for the repetitive insert sub-transitions in Figure 4 without adjustment by the open diamonds and squares for end- and loop-melting, respectively. Observed and calculated transition curves for the 228 bp insert in pN/MCS8 from lambda DNA, obtained at the $[Na^+]$ extremes of 0.0344 and 0.1139 M Na^+, are shown together in Figure 8. In all six examples, the agreement between observed and calculated T_M, transition amplitudes, breadths and areas is good, and the rms error small. Calculated T_M for other sequence domains are listed in column six in Table 1, with ΔT_M for the differences for loops listed in column nine, and represented by the dotted line in Figure 5. This agreement substantiates the several assumptions above, including the two-state assumption. Calculated denaturation maps also indicate that repetitive domains dissociate as loops in two-state fashion. Small differences between observed and calculated temperature scales are attributed to small errors in the experimental curves, or small uncompensated errors in $\Delta H_{ij}/\Delta S_{ij}$ for one or more of the 10 nearest neighbors (23).

DISCUSSION

Accurate T_{ij} and ΔH_{ij} have been obtained in this study from a systematic analysis of high-resolution melting curves of well-behaved synthetic tandemly repeating sequences over the range 0.034–0.114 M Na^+. The polymeric DNA specimens were recombinant plasmids, constructed with repetitive sequence inserts at a site with favorable energetic characteristics and convenient restriction sites for the linearization of plasmids in preparation for melting.

T_{ij} differ from those obtained in previous studies (14–18), as is apparent from free energy differences in Table 2b. Standard errors ($\pm 0.2°$) are significantly less than they were in our previous study (17), although magnitudes of T_{ij} remain in the same order by ***ij*** as reported in previous studies, with similar relationships of stacked purines and pyrimidines,

$$\delta\Delta\overline{G}_{pu \cdot py}\,(-397\text{ cal}) > \delta\Delta\overline{G}_{pu \cdot pu}\,(+30\text{ cal}) > \delta\Delta\overline{G}_{py \cdot pu}\,(+351\text{ cal}),$$

reflecting differences in stacking interactions for purine–pyrimidine, pyrimidine–purine and purine–purine neighbors. Results are consistent with neighbor-pair thermodynamic additivity (35), and the absence of any longer-range energetic factors, despite implications that might be interpreted to the contrary (36). The stability constant for entire domains depends only and quantitatively on the product of stability constants for each individual pair in domains, s_{ij}^N.

Transition enthalpies were determined by analysis of two-state equilibria associated with the melting of internal domains. The repetitive domains, locked in between two stable (G+C)-rich neighboring domains, are shown by several criteria to melt in two-state fashion when linearization is catalyzed by *Eco*RV, forcing domains to melt as closed loops. Average errors of ΔH_{ij} are approximately ±5%, slightly larger for domains of high $f_{(G+C)}$. ΔH_{ij} were verified from a systematic investigation of variations of T_{ij} with [Na^+], which depend inversely on ΔH_{ij} (12,32). Verified ΔH_{ij} increase with T_{ij}, in close agreement with the empirical function: $\Delta H_{ij} = 52.78 \cdot T_{ij}^{0.0745\,M-Na^+} - 9489$, and in parallel with a small increase in ΔS_{ij} (Table 2a), which varies with $T_{ij}([Na^+])$. ΔH_{ij} increases more-or-less in parallel with the (G+C) content of neighbor pairs, a reflection of increases in neighbor-dependent stacking and hydrogen bonding (37). Small variations in entropy with T_{ij} and $f_{(G+C)}$ appear to reflect variations in residual stacking in the dissociated coil state, and thereby, of variations in base hydration.

From a combination of replicate measurements and [Na^+]-dependent results, accuracies of ΔH_{ij} in Table 2a are approximately ±290 cal/mol bp, or ±4%, slightly larger for domains of highest $f_{(G+C)}$. Comparisons can be made with the results of an extensive compilation of calorimetric enthalpies and accompanying melting temperatures assembled by Klump (13), for a large number of natural and synthetic DNAs. Calorimetric transition enthalpies and entropies were summarized by the expressions:

$$\Delta H_{cal} = 7.63(1 + 0.235 \cdot f_{G+C}) \text{ kcal/mol bp} \quad \textbf{11}$$

$$\Delta S_{cal} = 23.62(1 + 0.055 \cdot f_{G+C}) \text{ cal/(mol bp} \cdot \text{deg)} \quad \textbf{12}$$

while the corresponding melting temperatures were fit to the following expression:

$$T_M = 50 + 55 \cdot f_{G+C}\,^{\circ}\text{C}. \quad \textbf{13}$$

Substituting **13** into **11** and **12** leads to:

$$\Delta H_{cal} = 32.6 \cdot T_M - 2905 \text{ cal/mol bp} \quad \textbf{14}$$

$$\Delta S_{cal} = 0.0236 \cdot T_M - 16.0 \text{ cal/(mol bp} \cdot \text{deg)} \quad \textbf{15}$$

Substituting T_{ij} for T_M leads to the values for $\Delta H_{cal,ij}$ and $\Delta S_{cal,ij}$ listed in the last two columns of Table 2a. ΔH_{ij} and ΔS_{ij} are in excellent agreement with $\Delta H_{cal,ij}$ and $\Delta S_{cal,ij}$, respectively, when the Klump results are presented in this fashion. Although stated that the transition entropy is independent of the sequence (13), values of both ΔS_{ij} and $\Delta S_{cal,ij}$ are seen to increase slightly with $T_{ij}([Na^+])$ and f_{G+C} of the neighbor pair.

Neighbor-pair additivity was also observed for (dA · dT)-tracts, where a plot of T_M of insert domains against the mole fraction of AA (TT) neighbor pairs they contain, f_{AA}, is linear (r = –0.9997). The absence of curvature or deviation at these higher temperatures suggests (dA · dT)-tracts no longer possess the unique structural features that characterize these tracts at lower temperatures (38–45): large propeller twists of the A · T pair, with three-centered hydrogen bonding and a narrow minor groove with a structural scaffolding provided by (dA · dT)-tract-associated bound water. These results are therefore complementary to those of Chan *et al.* (20,21), who found that the global melting of an oligomeric specimen with four equi-spaced (dA · dT)-tracts is preceded by a modest transition below 37°C, reflecting a pre-melting structural rearrangement of the tracts from a low temperature conformational state to the standard B-form at higher temperatures. The melting of oligomeric specimens used for measurements of calorimetric ΔH_{ij} often occur at <37°C, and therefore could reflect both pre-melting and global contributions.

The plot of T_M of (dA · dT)-tract-containing domains against f_{AA} extrapolates to 66.81° for the AA (TT) neighbor, in good agreement with that obtained by LU decomposition, 66.77°, but significantly higher than the T_M for poly(dA · dT), 65.45°C. The lower T_M for the latter reflects the increased access of long (dA · dT)-tracts to greater degrees of pairing freedom during melting, with sliding degeneracy and mismatched loops, (46) and thereby of a larger transition entropy than given in Table 2a for ApA.

The energetic effects of loops were determined from pN/MCS plasmids linearized in preparation for melting by *Eco*RV, which cleaves the DNA 805 bp away from the insert. The insert is isolated by (G+C)-rich barrier domains on both sides (Fig. 1), forcing it to melt as an internal loop. T_M for these interior 'loop domains' are higher than for 'end domains' of the same sequence, reflecting the stabilizing effects of base proximity in loops. While domain T_M of repetitive inserts at the end of helices are dependent only on sequence, they are dependent on both sequence and length when positioned internally. It was found that loop energy could be quantitatively defined by unique values for the cooperativity, loop exponent and stiffness parameters, applicable to internal domains of all sizes and sequence. The cooperativity parameter, $\sigma_c = 1.26 \times 10^{-5}$ is slightly larger than reported in our previous study (47).

Statistical mechanical curves computed with this value for the cooperativity parameter, and with $T_{ij}([Na^+])$ and ΔH_{ij} in Table 2, are in quantitative agreement with observation: in T_M, transition amplitudes, breadths and areas of domain sub-transitions. With accurate values of T_{ij} and ΔH_{ij} it is possible to calculate accurate stabilities of different sequences without recourse to actual melting experiments. A program called MELTSIM has been developed for use in the windows operating system for calculating melting curves and denaturation maps of polymeric DNA sequences, and will be made available by anonymous ftp.

ACKNOWLEDGEMENTS

We gratefully acknowledge Colin McRavey for his excellent assistance in the sequencing of DNAs and for his valuable contributions to discussions and a spirited laboratory environment. We also acknowledge Calvin Mitchell III, for his expert assistance in the development of appropriate statistical methods of analyses. Supported in part by grants from MAES (project no. 08402) and NIH.

REFERENCES

1 Crothers, D.M. (1968) *Biopolymers* **6**, 1391–1404.
2 Vizard, D., White, R. and Ansevin, A.T. (1978) *Nature* **275**, 250–251.
3 Blake, R.D. and Lefoley, S.G. (1978) *Biochim. Biophys. Acta* **518**, 233–246.
4 Breslauer, K.J., Frank, R., Blöcker, H. and Marky, L.A. (1986) *Proc. Natl. Acad. Sci. USA* **83**, 3746–3750.
5 Breslauer, K.J. (1986) In Hinz, H.-J. (ed.), *Thermodynamic Data for Biochemistry and Biotechnology.* Springer-Verlag, Berlin, chapter 15, pp. 402–427.

6 Sugimoto, N., Nakano, S., Yoneyama, M. and Honda, K. (1996) *Nucleic Acids Res.* **24**, 4501–4505.
7 SantaLucia, J., Jr, Allawi, H. and Seneviratne, P.A. (1996) *Biochemistry* **35**, 3555–3562.
8 Krakauer, H. and Sturtevant, J.M. (1968) *Biopolymers* **6**, 491–512.
9 Privalov, P.L., Ptitsyn, O.D. and Birshtein, T.M. (1969) *Biopolymers* **8**, 559–571.
10 Klump, H. and Ackermann, T. (1971) *Biopolymers* **10**, 513–522.
11 Shiao, D.D.F. and Sturtevant, J.M. (1973) *Biopolymers* **12**, 1829–1836.
12 Record, M.T., Anderson, C.F. and Lohman, T.M. (1978) *Q. Rev. Biophys.* **11**, 103–178.
13 Klump, H.H. (1988) In Jones, M.N. (ed.), *Biochemical Thermodynamics*. 2nd edition. Elsevier Press, Amsterdam, pp. 100–144.
14 Gotoh, O. and Tagashira, Y. (1981) *Biopolymers* **20**, 1033–1042.
15 Gotoh, O. (1983) *Adv. Biophys.* **16**, 1–52.
16 Wartell, R.M. and Benight, A.S. (1985) *Phys. Rept* **126**, 67–107.
17 Delcourt, S.G. and Blake, R.D. (1991) *J. Biol. Chem.* **266**, 15160–15169.
18 Doktycz, M.J., Goldstein, R.F., Paner, T.M., Gallo, F.J. and Benight, A.S. (1992) *Biopolymers* **32**, 849–864.
19 Blake, R.D. (1996) In Meyers, R.A. (ed.), *Encyclopedia of Molecular Biology and Molecular Medicine*. Vol. 2. VCH Verlagsgesellschaft mbH, Weinheim, FRG, New York, pp. 1–19.
20 Chan, S.S., Breslauer, K.J., Austin, R.H. and Hogan, M.E. (1993) *Biochemistry* **32**, 11776–11784.
21 Chan, S.S., Austin, R.H., Mukerji, I. and Spiro, T.G. (1997) *Biophys. J.* **72**, 1512–1520.
22 Yen, S.-W.W. and Blake, R.D. (1981 *Biopolymers* **20**, 1161–1181.
23 Blake, R.D. and Delcourt, S.G. (1996) *Nucleic Acids Res.* **24**, 2095–2103.
24 Maniatis, T., Fritsch, E.F. and Sambrook, J. (1982) *Molecular Cloning: A Laboratory Manual*, Cold Spring Harbor Laboratory Press, Cold Spring Harbor Laboratory, New York, NY.
25 Zhang, H., Scholl, R., Browse, J. and Somerville, C. (1988) *Nucleic Acids Res.* **16**, 1220.
26 Yen, S.-W.W. and Blake, R.D. (1980) *Biopolymers* **19**, 681–700.
27 Blake, R.D. and Hydorn, T.G. (1985) *J. Biochem. Biophys. Methods* **11**, 307–316.
28 Blake, R.D., Vosman, F. and Tarr, C.E. (1981) In Sarma, R.H. (ed.), *Proc. 2nd SUNYA Convers. Disc. Biomol. Stereo.* Vol 1. Adenine Press, NY. pp. 439–458.
29 Press, W.H., Flannery, B.P., Teukolsky, S.A. and Vetterling, W.T. (1986) *Numerical Recipes*, Cambridge University Press, NY, pp. 31–43.
30 Marmur, J. and Doty, P. (1959) *Nature* **183**, 1427.
31 Schildkraut, C.L., Marmur, J. and Doty, P. (1962) *J. Mol. Biol.* **4**, 430–443.
32 Manning, G.S. (1978) *Q. Rev. Biophys.* **11**, 179–246.
33 Filimonov, V.V. and Privalov, P.L. (1978) *J. Mol. Biol.* **122**, 465–470.
34 Klotz, L.C. (1969) *Biopolymers* **7**, 265–273.
35 Dill, K.A. (1997) *J. Biol. Chem.* **272**, 701–704.
36 Dickerson, R.E. (1992) *Methods Enzymol.* **211**, 67–110.
37 Friedman, R.A. and Honig, B. (1995) *Biophys. J.* **69**, 1528–1535.
38 Wu, H.-M. and Crothers, D.M. (1984) *Nature* **308**, 509–513.
39 Diekmann, S. and Wang, J.C. (1985) *J. Mol. Biol.* **86**, 1–11.
40 Hagerman, P.J. (1986) *Nature* **321**, 449–450.
41 Nelson, H.C.M., Finch, J.T., Luisi, B.F. and Klug, A. (1987) *Nature* **330**, 221–226.
42 Coll, M., Wang, C.A.-J. and Rich, A. (1987) *Proc. Natl. Acad. Sci. USA* **84**, 8385–8389.
43 Yoon, C., Prive, G.G., Goodsell, D.S. and Dickerson, R.E. (1988) *Proc. Natl. Acad. Sci. USA* **85**, 6332–6336.
44 Aymami, J., Coll, M., Frederick, C.A., Wang, A.H.-J. and Rich, A. (1989) *Nucleic Acids Res.* **17**, 3229–3245.
45 DiGabriele, A.D., Sanderson, M.R. and Steitz, T.A. (1989) *Proc. Natl. Acad. Sci. USA* **86**, 1816–1820.
46 Applequist, J. (1969) *J. Chem. Phys.* **50**, 600–609.
47 Blake, R.D. and Delcourt, S.G. (1987) *Biopolymers* **26**, 2009–2026.